JOURNAL OF THERMOPHYSICS AND HEAT TRANSFER
Vol. 7, No. 1, Jan.–March 1993

Comparison of Theory with Experiment for the Bow Shock Ultraviolet Rocket Flight

D. A. Levin*
Institute for Defense Analyses, Alexandria, Virginia 22311
G. V. Candler†
North Carolina State University, Raleigh, North Carolina 27695
R. J. Collins‡
University of Minnesota, Minneapolis, Minnesota 55455
P. W. Erdman§ and E. Zipf¶
University of Pittsburgh, Pittsburgh, Pennsylvania 15260
and
P. Espy** and C. Howlett††
Utah State University, Logan, Utah 84322

Comparison is made between the results obtained from a state-of-the-art thermochemical nonequilibrium flowfield and radiation code and data obtained from a recent experiment. The experiment obtained the first measurements of ultraviolet radiation from the shock-heated gas in the nose region of a 0.1016-m nose radius vehicle traveling at about 3.5 km/s at altitudes between 37–75 km. The preflight computations agree at low altitudes but underpredict the data at high altitudes. Postflight flowfield and radiation sensitivity studies suggest improvements for the models at high altitudes. Specifically, excitation mechanisms that contribute to production of NO gamma-band emission need to be revised. Altitude dependence of the radiation observed from the OH radical can be understood in terms of nonequilibrium chemistry in the flow.

Introduction

THERE has been a recent effort to study the thermophysics of shock-heated air in the vicinity of the nose of a slender vehicle flying at about 3.5 km/s. Two recent articles represent an effort to predict the radiation emission from this type of flowfield.[1,2] This work relied on the numerical technique of Candler[3] to predict the flowfield characteristics and the nonequilibrium air radiation (NEQAIR) program of Park[4] to assess the radiative emission. Using these results, a rocket experiment was designed to measure ultraviolet emission from these flows. This experiment, bow shock ultraviolet (BSUV), was successfully flown in April 1990. A more lengthy discussion of the payload instrument characteristics and trajectory may be found in Ref. 5. The results discussed here correspond to a constant speed of 3.5 km/s at altitudes from 37 to 75 km.

The computational technique that was used to predict the flowfield models air as composed of seven chemical species (N_2, O_2, NO, NO^+, N, O, and e$^-$).[6] These chemical species are allowed to react with each other at finite rates. It is assumed that the temperature that governs the vibrational and electron translational energy modes T_v may be different than the heavy particle translational-rotational temperature T. This model will be designated throughout this article as the "baseline multi-T model." Additionally, in the radiation model it is assumed that T_v is the temperature that controls the population of the excited electronic states. These models have been tested at various flight conditions and have been shown to give good comparisons to other experimental data.[6,7] Generally, however, the experimental data that have been used in the past have been at speeds of 5 km/s and higher and have provided data for parameters that are not especially sensitive to the thermochemical model (e.g., surface pressure and heating rates). The data from this flight are considered to be highly reliable and serve as a good test of the thermophysical model in the 3.5 km/s flight regime. To determine an upper limit on the radiation within the context of the preflight flowfield and radiation models, emissions were calculated using a variant of the original baseline multi-T model. The heavy particle translational-rotational temperature and the electron-vibrational temperature were assumed to be equilibrated. (Chemical nonequilibrium was maintained.) The radiation model was used as before, except that this single temperature was the controlling temperature. The preflight results from this model will be designated as the "single-T" model.

It is the purpose of this article to assess the success of the computational techniques in terms of preflight predictions of the flowfield and levels of radiative emission in the 190–400-nm spectral region. It will be seen that the comparison is fairly good for the lower portion of the trajectory, but that it is poor for the higher altitudes. At lower altitudes the signal magnitudes were in agreement with preflight calculations[2] and ground-based shock tube work.[8] Flight spectra showed emissions from expected molecular systems, i.e., NO and OH. This article will discuss enhancements to the models subsequent to the flight that provide better agreement at higher altitudes.

The present models have no predictive capability to model radiation from the OH radical which was observed during the flight. Using a quasisteady state assumption, the flowfield

Presented as Paper 91-1411 at the AIAA 26th Thermophysics Conference, Honolulu, HI, June 24–26, 1991; received Dec. 4, 1991; revision received March 2, 1992; accepted for publication March 3, 1992.

*Research Staff, Science and Technology Division. Member AIAA.
†Assistant Professor, Department of Mechanical and Aerospace Engineering. Member AIAA.
‡Professor, Department of Electrical Engineering.
§Research Associate, Department of Physics and Astronomy.
¶Professor, Department of Physics and Astronomy. Member AIAA.
**Research Associate Professor, Department of Physics.
††Technical Program Manager, Center for Space Engineering. Member AIAA.

temperature and density were used in conjunction with kinetic analyses to explain the altitude-dependence of that signal.

Comparison of Experiment and Preflight Models

Figure 1 shows the relative signal strength of the shock-heated gas as a function of time after launch. The photometer is centered at 230 nm, has a bandwidth of 51 nm, and views the stagnation region through a conformal fused silica window. The radiation is dominated by the NO ($A \rightarrow X$ transition) gamma-band system in this spectral region. Absolute calibration of these data[5] provides a signal level of 0.014 W/cm^2-μsr at 40 km which is a factor of two lower than either the baseline multi-T or single-T model. At lower altitudes the analog data curve represents the best detector response. The orders of magnitude discrepancy between the baseline multi-T model and experiment at higher altitudes is apparent. The single-T model is seen to agree well with the data, especially at higher altitudes.

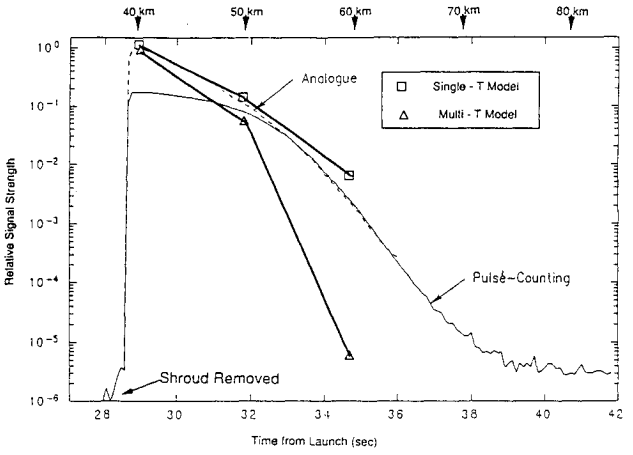

Fig. 1 Comparison of on-axis photometer relative signal strength with "single-temperature" and "multiple-temperature" models as a function of altitude.

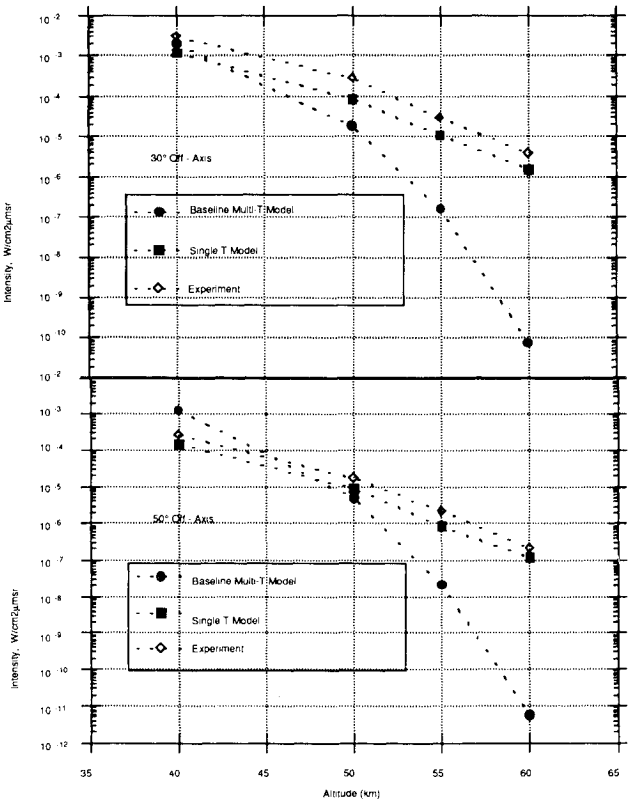

Fig. 2 Off-axis radiometer and model comparisons.

In Fig. 2 comparison with the theory is given for the off-axis NO photometers.[5] The baseline multi-T calculations predicted signal levels that would not have been observable by the off-axis photometers for altitudes higher than 50 km.[2] However, the data show that the signal falls off with angle more slowly than predicted by the baseline multi-T theory. Again, the single-T model is seen to agree well with the data at the higher altitudes.

A series of spectra obtained with the forward-viewing spectrometer is shown in Fig. 4 of Ref. 5. The spectra show that the dominant radiator is NO; the N_2^+ band structure is not visible in this flight regime. At longer wavelength the emergence of the OH ($X \rightarrow A$) peak at 310 nm above the continuum of the NO gamma-band structure is observed, particularly at higher altitudes. The OH signal will be shown to be due to the presence of water in the atmosphere. It also serves to provide additional confirmation of the mechanism for populating the upper electronic states of heteronuclear diatomic species.

Enhancements to the Flowfield Model

Comparison of experiment with preflight model predictions shows that the single-T model appears to better predict radiance levels than the multi-T model. In this flight regime, however, there are insufficient numbers of collisions for the gas to reach vibrational-translational equilibrium.[9] Therefore, a single-T model is physically incorrect with fortuitous experimental agreement. The discrepancy between the experiment and the baseline multi-T model may arise in either the flowfield or radiation modeling, or both. In this article we primarily consider improvements to the baseline multi-T model that account for rarefication effects,[10,11] deviations from the Millikan and White[12] vibrational relaxation rates, and numerical accuracy. The last change was achieved through incorporation of an adaptive grid technique.[13] The inclusion of rarefication effects and the improvements to the Millikan and White relaxation rates will be discussed below.

There are several reasons why the baseline flowfield model could break down at high altitudes where rarefaction effects start to become important. In this portion of the trajectory, the freestream mean-free-path approaches the shock standoff distance. There are three primary rarefaction effects that must be considered. First, the linear variation of stress with strain and heat flux with temperature gradient may break down. This results in thicker shock waves than predicted by the Navier-Stokes equations. The second effect is the presence of rotational thermal nonequilibrium. That is, the rotational temperature is different than the translational temperature for significant portions of the flowfield. Thirdly, there may be velocity and temperature slip at the body surface. In this work, we have included the first two effects, and neglected the third because the radiative emission is unaffected by the conditions near the body surface. Therefore, the exact details of the flow in the near-wall region do not affect the comparison to the experiment.

The effects of the nonlinear variation of stress with strain and heat flux with temperature are included through the use of the simplified translational nonequilibrium model (STNM) of Lumpkin.[11] In Lumpkin's work several of the important terms in the Burnett equations were included in one-dimensional flowfield computations. These terms were shown to accurately reproduce the full Burnett equation results. This approach was taken in this work so that the effects of the thick shocks could be included without a large amount of computational effort. The stress tensor and the heat flux vector are modified to have the form

$$\tau_{ij} = -2\mu\left(D_{ij} - \frac{1}{3}D_{kk}\delta_{ij}\right) + \varpi\frac{3}{2}\frac{\mu^2}{p}\frac{\partial u_k}{\partial x_k}\left(D_{ij} - \frac{1}{3}D_{kk}\delta_{ij}\right) \quad (1)$$

$$q_i = -\kappa_t \frac{\partial T}{\partial x_i} + \vartheta \frac{\mu^2}{\rho T} \frac{\partial T}{\partial x_j} \frac{\partial u_k}{\partial x_k} \tag{2}$$

where D_{ij} is the strain rate tensor

$$D_{ij} = \frac{1}{2}\left(\frac{\partial u_i}{\partial x_j} + \frac{\partial u_j}{\partial x_i}\right) \tag{3}$$

and ϖ and ϑ are constants defined in Ref. 11, and were chosen to be $\varpi = 8$ and $\vartheta = 11.231$.

The effects of rotational thermal nonequilibrium were modeled using the loaded sphere model of Jeans.[14] Coupling this model with the conservation equation for rotational energy, yields the equation

$$\frac{\partial E_r}{\partial t} + \frac{\partial E_r u_j}{\partial x_j} = -\sum_{s\ \text{rot}} \frac{\partial E_{rs} v_{sj}}{\partial x_j} + \sum_{s\ \text{rot}} \frac{E_{rs}^*(T) - E_{rs}}{\tau_{rs}} + \sum_{s\ \text{rot}} \frac{E_{rs} w_s}{\rho_s} \tag{4}$$

where E_{rs} is the rotational energy of species s per unit volume, E_r is the total rotational energy per unit volume, * represents the value at equilibrium, v_{sj} is the diffusion velocity of species s, and τ_{rs} is the rotational relaxation time. This is the product of the rotational collision number Z_{rs} and the mean collision time τ_{cs}. The rotational collision number is obtained from the theory of Parker.[15] w_s is the rate of change of species s density due to chemical reactions. Note that this model does not include any explicit rotation-vibration coupling. However, rotation is effectively coupled to vibration through translation-rotation and translation-vibration energy exchange mechanisms.

The rotational energy conservation equation is solved along with the other conservation equations for mass, momentum, vibrational energy, and total energy. The effects of rotational nonequilibrium may be seen in Fig. 3, which is a plot of the temperatures along the stagnation streamline for a 10.16-cm nose radius body traveling at 3.5 km/s and 50-km altitude. For these conditions, the rotational nonequilibrium region is about 0.4 cm, and the vibrational nonequilibrium region is about 1.0 cm.

The second important change to the baseline flowfield model was the use of improved vibrational relaxation rates. The baseline version of the multi-T model assumed the following semi-empirical form for vibrational relaxation[12]:

$$\tau_{rs} p = \exp[A_{rs}(T^{-1/3} - 0.015\mu_{rs}^{1/4}) - 18.42] \quad \text{(atm-s)} \tag{5}$$

$$A_{rs} = 1.16 \times 10^{-3} \mu_{rs} \theta_{vs}^{4/3} \tag{6}$$

where τ_{rs} is the vibrational relaxation time of species r due to collisions with species s, p is the gas pressure, T is the heavy particle translational temperature, μ_{rs} is the reduced mass, and θ_{vs} is the characteristic temperature of vibration. The N_2-NO, N_2-O_2, O_2-O, NO-NO, NO-O, and N_2-O interactions have been shown to deviate significantly from the Millikan and White semiempirical vibrational relaxation rates.[9] Table 1 lists the new set of parameters used, A' and B', which were determined by curve-fitting the data from the respective sources. The relative change in relaxation rates obtained using the values given in Table 1 and Eq. (5) can be seen to be largest at the lower temperatures and are significant in the temperature range of interest here ($T \approx 6000$ K).

The results of the modifications to the baseline model are shown in Figs. 4 and 5. Figure 4 shows the heavy particle translational temperature as a function of each change, and the total change. Each change has the effect of raising that temperature immediately after the shock, with the total change increasing to about 1100 K above the baseline calculation. The maximum value of the heavy particle translational temperature is most sensitive to the incorporation of rotational nonequilibrium. The translational temperature over most of the shock layer was found to be insensitive to any of the changes made. The effects of the corresponding modifications on the vibrational temperature are shown in Fig. 5. In contrast to the translational temperature, the vibrational temperature is affected most by the corrections to the Millikan and White

Table 1 Modified vibrational relaxation parameters[a]

System	Source	A'	B'	A_{rs}
N_2-O_2	Breshears et al.[16]	115.1	19.45	228.7
N_2-NO	Taylor et al.[17]	101.2	17.79	225.3
N_2-O	McNeal et al.[18]	31.06	16.04	188.9
O_2-O	Kiefer et al.[19]	43.56	21.03	111.0
NO-NO	Wray[20]	63.28	22.03	178.7
NO-O	Kiefer et al.[19]	43.56	21.03	149.1

[a] $\tau_{rs} p = \exp(A' T^{-1/3} - B')$, atm-s.

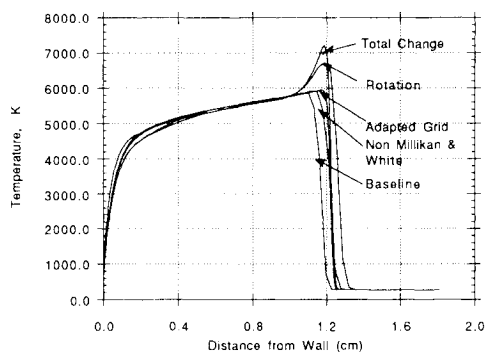

Fig. 4 Comparison of predicted heavy particle temperatures for different flowfield models.

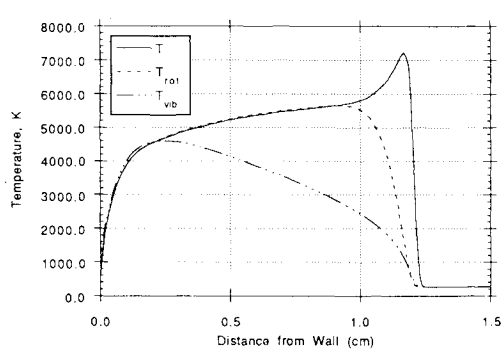

Fig. 3 Comparison of temperatures for 50 km, 3.5 km/s and 0.1016-m nose radius.

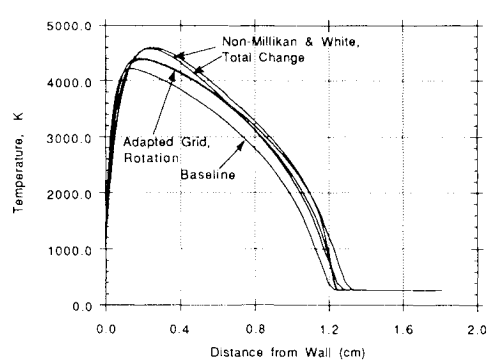

Fig. 5 Comparison of predicted vibrational temperatures for different flowfield models.

rates. The number density of NO formed in the shock layer did not change appreciably from the baseline calculation for any of the modifications discussed above.

Comparison of New Calculations with Experimental Radiation Results

Figures 6–8 show the results obtained by using the enhanced multi-T model. In these plots NEQAIR has been used in two different ways. First consider the results obtained by running NEQAIR as originally formulated by Park.[4] The figures show radiation centered at 230 nm with a filter full-width at half-maximum of 51 nm for angles of 0, 30, and 50 deg from the stagnation streamline. The data have been integrated over a time period of 0.25 s which represents an altitude resolution of 870 m. The NEQAIR-generated spectral radiance was convolved with the calibrated photometer filter functions. All three viewing angles show similar signal vs altitude trends, namely the computed results agree well at low altitude, but are many orders of magnitude in error at high altitude.

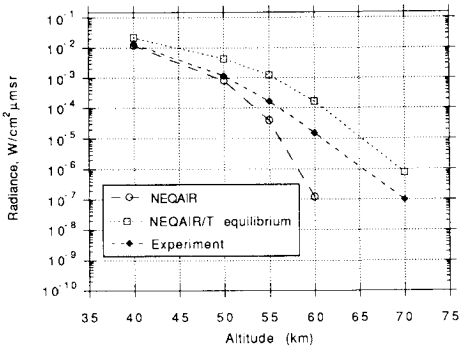

Fig. 6 Final flowfield and radiance model comparison with experiment. Forward viewing 0 deg.

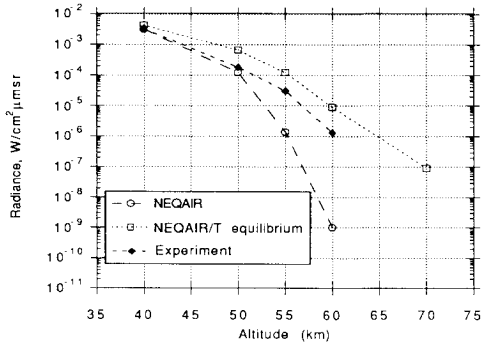

Fig. 7 Final flowfield and radiance model comparison with experiment. Forward viewing 30 deg.

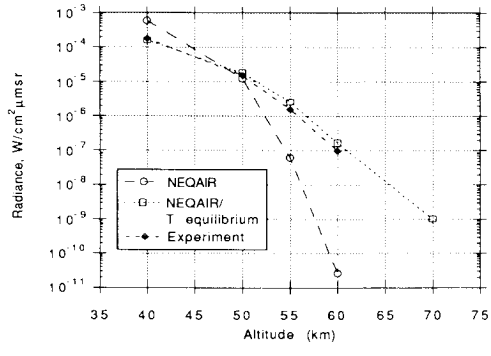

Fig. 8 Final flowfield and radiance model comparison with experiment. Forward viewing 50 deg.

The small deviation in that trend seen in Fig. 8 (50-deg viewing) is probably due to rocket precession (of about a 1-s period) that has not been removed from the data. The agreement between the experiment (enclosed diamonds) and the enhanced flowfield with the NEQAIR model (open circles) remains poor at altitudes above 50 km. Moreau et al.[21] obtained similar comparison between flight data and their flowfield and radiance calculations.

The lack of agreement with the experiment caused us to consider whether there were inadequacies in the NEQAIR model itself. The NEQAIR model was originally developed and used in a higher speed flight regime where the primary radiating band system studied was N_2^+ first negative. Under these conditions electron impact excitation mechanisms dominate and have therefore been tested more carefully than neutral impact excitation mechanisms. The model assumes that a pure Boltzmann treatment is not correct; yet, there are sufficient collisions to arrive at a quasisteady state. The quasisteady state formalism requires excitation cross sections which may be in error from the values presently in the model. Recent laser-induced quenching experiments[22] in NO and N_2 have indicated that the excitation cross section may be a factor of 50 higher than previously thought. It has also been assumed that the coupling between the first (A) and second electronic (B) states of NO is stronger than with the ground state. In addition, the role of the heavy particle and vibrational temperatures in the radiation model has also come under question. Assumptions such as these must now be reviewed more closely before a full correction to the radiation model is made.

To give an indication of the sensitivity of the predicted radiation to the assumptions in NEQAIR a third curve designated "NEQAIR/T equilibrium" (open squares) has been plotted. These results were obtained using the enhanced multi-T flowfield model in conjunction with NEQAIR except that the way NO radiation is computed has been changed. For the NO molecular system the electronic state populations have been calculated assuming a Boltzmann distribution with the governing temperature assumed to be the flowfield heavy particle temperature. Using the upper state distribution derived in this manner, the spectral radiance is calculated with the present NEQAIR atomic and molecular spectroscopic constants. Comparison of this result with an experiment for all three viewing angles shows that a Boltzmann assumption is not correct since a factor of about five more radiation is predicted than was observed. However, the Boltzmann assumption shows a significantly slower decrease with altitude than the unmodified NEQAIR curve.

This simple modification to NEQAIR demonstrates that the approach taken to modeling the radiation is critical while improvements to the flowfield modeling are less important for these flow conditions. It would appear that the population of the NO excited states is more closely linked to the translational temperature than was previously thought. Analyses presented in the next section for another molecular system support that conclusion as well.

Analysis of Observed OH Radiation

As mentioned earlier, radiation from the first excited state to the ground electronic state of the OH radical system was observed in spectrometer scan traces at higher altitudes. At the lowest altitude the OH peak is barely discernible compared to the background level of the NO gamma and beta-band system. However, by 63 km the OH system is clearly resolved (see Fig. 4 of Ref. 5). In the discussion below, a model for the OH radiation will be presented based on the assumption that the source of OH is water present in the ambient atmosphere. The analysis will focus on the relative spectral intensity of OH and NO radiation which will be shown to be consistent with the nonequilibrium nature of the flow. The rate of production of OH and NO will be compared for density and temperature values appropriate to the flight conditions. The comparisons will be based on solutions of an

augmented set of rate equations made using a code for reaction chemistry, "CHEMKIN."[23] The assumption that the ratio of NO to OH concentrations can be considered without recomputing the flow for the case containing water is justified since trace amounts of an additional component do not significantly affect the energy balance, and therefore, will not change the density and temperature behind the shock.

Radiation from the OH system has been observed in other rocket flights during re-entry[1] and in ground-based shock tube measurements. In the former case the source may be due to outgassing from the payload, ambient atmospheric water, or both. In laboratory tests even trace amounts of water will dissociate and produce OH which can be observed with ease due to its strong oscillator strength. In the altitude region where data were obtained (37–75 km) the mixing ratio of ambient water is known[24] to be on the order of 10^{-5}–10^{-6}. Additional confirmation of the presence of OH radiation was obtained from a stagnation stream viewing radiometer.[5] Order of magnitude ground state OH radical concentration can be computed from that radiometer's signal as

$$n_X \cong \frac{I\tau\lambda}{\Delta x h c} \exp\left(+\frac{\Delta E}{kT}\right) \tag{7}$$

where n_x is the concentration of OH in the ground state, per cm^3; I is the signal in W/cm^2-sr; τ is the lifetime of the A state, 715 ns; λ is the central radiometer frequency, 0.310×10^{-6} m; h is Planck's constant, 6.63×10^{-34} J/s; c is the speed-of-light, 3×10^8 m/s; k is Boltzmann's constant, 0.69 cm^{-1}/K; ΔE is the energy spacing between the X and A state, 32,258 cm^{-1}; Δx is the approximate shock layer thickness, 1 cm; and T is the approximate upper state electronic temperature, 4830 K.

At 43 km (the lowest altitude after nose cone ejection induced transients) an intensity of 1.7×10^{-5} W/cm^2-sr was observed. This signal level used in conjunction with Eq. (6) gives a ground state OH concentration on the order of 3×10^{11}/cm^3 which when compared with the ambient atmospheric density of 8.5×10^{16}/cm^3 gives a mixing ratio on the order of 4×10^{-6}. The assumed approximate shock layer thicknesses, Δx and T, are consistent with Figs. 5 and 6.

Since our ultimate goal is to compare the ratio of NO-to-OH radiation in the near UV (λ = 310 nm), a more quantitative formalism than Eq. (7) is required to model the relative production rates of those species. The computation of the time-dependent concentrations of reacting species requires a solution of coupled rate equations. These reactions and their forward rates are given in Table 2.

The time-dependent solution of this reaction system based on kinetic data taken from Ref. 25 provided various insights into the shock-layer chemistry in this flight regime. For example, it was found that the chemical solutions were the same with and without the presence of water at a mixing ratio of 10^{-5}, i.e., mole fractions of major species such as N_2, O_2, NO, N, and O did not significantly change. Figures 9 and 10 give examples of two solutions of these equations obtained at pressures of 0.01 and 0.3 atm, respectively, and at a temperature of 4830 K. A total reaction time of 10 μs was used which corresponds to the time that the gas remains in the fields of view of the spectrometer and the forward-looking radiometer after entering the shock layer. In both cases the presence of OH emphasizes the chemical nonequilibrium aspect of the flow. At these temperature and pressure conditions a purely equilibrium calculation would predict total decomposition of water. The mole fractions of NO and OH (as shown in the figures) display a different time dependence that can be understood from review of the reactions used in the calculation (see Table 2). Formation of NO is the result of a reaction between N_2 and O which is a reaction product, making the formation of NO a two-step process. The formation of OH, however, is achieved by a single-step dissociation of H_2O. Clearly, while this major difference will not affect the equilibrium concentrations of OH and NO, it will influence their relative concentrations before equilibrium is reached. This effect is particularly apparent when comparing Figs. 9 (altitude >60 km) and 10 (altitude of about 40 km).

Figure 11 shows a plot of the ratio of NO-to-OH concentration as a function of shock-layer pressure with the shock-layer pressure-to-altitude correspondence also shown. The

Table 2 Chemical reactions used in CHEMKIN analyses

Reaction	C'_{fm}	η_m	E_m/R
Original set used in two-dimensional flowfield model[5]			
$N_2 + N_2 = N + N + N_2$	3.7E + 21	−1.6	223,004
$N_2 + O_2 = N + N + O_2$	3.7E + 21	−1.6	223,004
$N_2 + NO = N + N + NO$	3.7E + 21	−1.6	223,004
$N_2 + N = N + N + N$	1.1E + 22	−1.6	223,004
$N_2 + O = N + N + O$	1.1E + 22	−1.6	223,004
$N_2 + e = N + N + e$	8.30E + 24	−1.6	223,004
$N_2 + NO^+ = N + N + NO^+$	3.70E + 21	−1.6	223,004
$O_2 + N_2 = O + O + N_2$	2.75E + 19	−1.0	117,215
$O_2 + N = O + O + N$	8.25E + 19	−1.0	117,215
$O_2 + O_2 = O + O + O_2$	2.75E + 19	−1.0	117,215
$O_2 + NO = O + O + NO$	2.75E + 19	−1.0	117,215
$O_2 + e = O + O + e$	1.32E + 19	−1.0	117,215
$O_2 + NO^+ = O + O + NO^+$	2.75E + 22	−1.0	117,215
$O_2 + O = O + O + O$	8.2E + 19	−1.0	117,215
$NO + N_2 = N + O + N_2$	2.3E + 17	−0.5	148,375
$NO + O_2 = N + O + O_2$	2.3E + 17	−0.5	148,375
$NO + NO = N + O + NO$	2.3E + 17	−0.5	148,375
$NO + N = N + O + N$	4.6E + 17	−0.5	148,375
$NO + O = N + O + O$	4.6E + 17	−0.5	148,375
$NO + e = N + O + e$	7.36E + 19	−0.5	148,375
$NO + NO^+ = N + O + NO^+$	2.3E + 17	−0.5	148,375
$N_2 + O = NO + N$	1.8E + 13	0.1	74,269
$NO + O = O_2 + N$	2.16E + 8	1.29	37,863
$N + O = NO^+ + e$	6.5E + 11	0.0	63,040
Reactions added for water analyses[25]			
$O_2 + H = O + OH$	2.2E + 14	0.0	16,646
$H_2O + N_2 = H + OH + N_2$	3.5E + 16	0.0	100,510
$OH + N_2 = H + O + N_2$	7.5E + 14	0.06	100,470

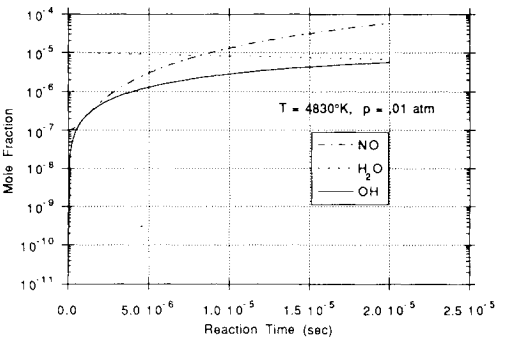

Fig. 9 Finite-rate kinetic solutions for gas conditions at T = 4830 K and P = 0.01 atm.

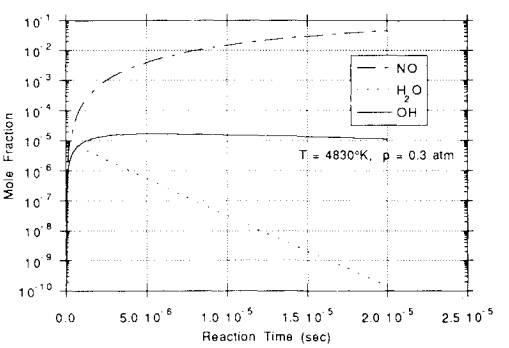

Fig. 10 Finite-rate kinetic solutions for gas conditions at T = 4830 K and P = 0.3 atm.

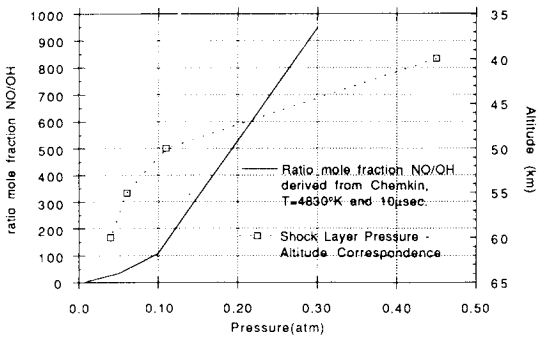

Fig. 11 Ratio of NO to OH relative concentration as a function of altitude.

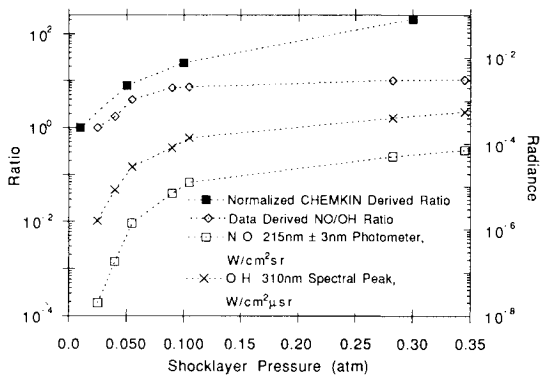

Fig. 12 Comparison of data with CHEMKIN model.

figure shows that at higher altitudes the NO-to-OH ratio decreases. Since the ratio of the spectral intensity of different components of an optically thin gas is directly related to their relative concentrations, the calculated variation of the ratio of NO to OH with altitude is in agreement with spectrometer observations.

The NO-to-OH ratio was calculated from the data as follows. The OH signal was calculated as the difference between the peak height at 310 nm and the local background, which was assumed due to the NO gamma, beta, and O_2 Schumann-Runge band continuum. The NO signal level was taken from the narrow band forward-looking NO photometer[5] centered at $\lambda = 215 \pm 3$ nm. Figure 12 shows the normalized ratio of the NO-to-OH peak as a function of pressure in the shock layer derived from the experiment compared with the CHEMKIN calculations. The individual measurement values obtained from the spectrometer and radiometer are also shown. The offset between the two curves may be arbitrarily set. Thus, the same shape of the curves shows reasonably good agreement between experiment and calculation. Deviations at higher shock-layer pressures (i.e., lower altitudes) are probably due to the difficulty of separating OH from the background NO signal.

Conclusions

The BSUV experiment has provided the first spectrally resolved data in the flight regime of 3.5 km/s speed from altitudes of 37–75 km. Excellent agreement between modeling and experiment at 40 km was crucial to permit an accurate setting of instrument sensitivity levels[5] and to provide confidence in higher altitude results. The persistence of ultraviolet signals in the NO gamma bands at higher altitudes than predicted preflight suggests that improvements are required in the flowfield and radiation modeling. Subsequent enhancements to the flowfield modeling have been made to account for thick shock waves, rotational nonequilibrium, better grid resolution, and more accurate vibrational-translational relaxation rates. These enhancements coupled with the NEQAIR model did not significantly improve agreement with an experiment at the higher altitudes. While a Boltzmann description of the NO excited states provides better altitude trends, individual altitude agreement is about a factor of five too high. Work is required to incorporate better excitation cross sections for the NO system and to insure that the dominant excitation/deexcitation paths are modeled correctly.

The study of another molecular system, OH, independently suggests that the heavy particle temperature controls the upper electronic state populations of simple heteronuclear diatomic systems. The spectrometer and photometer observations confirmed the atmospheric data that lists water as a trace species in the altitude regime where measurements were obtained. The analyses support the interpretation that OH radiation is due to shock-heated ambient water and not outgassing from the payload. The presence of OH in the flow underscores its chemical nonequilibrium nature. The altitude dependence of NO-to-OH radiation signal levels distinctly illustrates the two-step vs single-step production mechanisms of those two molecular systems.

Acknowledgments

This research is supported by SDIO/IST managed by the Army Research Office under Contract MDA903-89-C-0003. We would also like to acknowledge the computational chemistry Branch of NASA Ames Research Center for providing supercomputer time.

References

[1]Levin, D. A., Loda, R. T., Candler, G. V., and Park, C., "Theory of Radiation from Low Velocity Shock Heated Air," AIAA Paper 90-0312, Jan. 1990.

[2]Levin, D. A., Collins, R. J., and Candler, G. V., "Computations for Support Design of Measurements of Radiation from Low Velocity Shocked Air," *Journal of Thermophysics and Heat Transfer*, Vol. 5, No. 4, 1991, pp. 463–468.

[3]Candler, G. V., "The Computation of Weakly Ionized Hypersonic Flows in Thermo-Chemical Nonequilibrium," Ph.D. Dissertation, Stanford Univ., Stanford, CA, 1988.

[4]Park, C., "Calculation of Nonequilibrium Radiation in the Flight Regimes of Aero-Assisted Orbital Transfer Vehicles," *Thermal Design of Aero-Assisted Orbital Transfer Vehicles*, edited by H. F. Nelson, Vol. 96, Progress in Astronautics and Aeronautics, 1985.

[5]Erdman, P., Zipf, E., Espy, P., Howlett, C., Loda, R., Collins, R., Levin, D., and Candler, G., "Flight Measurements of Low Velocity Bow Shock Ultraviolet Radiation," AIAA Paper 91-1410, 1991.

[6]Candler, G. V., and MacCormack, R. W., "The Computation of Hypersonic Ionized Flows in Chemical and Thermal Nonequilibrium," *Journal of Thermophysics and Heat Transfer*, Vol. 5, No. 3, 1991, pp. 266–273.

[7]Candler, G. V., "On the Computation of Shock Shapes in Nonequilibrium Hypersonic Flows," AIAA Paper 89-0312, 1989.

[8]Wurster, W. H., Treanor, C., and Williams, M., "Non-Equilibrium UV Radiation and Kinetics Behind Shock Waves in Air," AIAA Paper 89-1918, June 1989.

[9]Park, C., *Nonequilibrium Hypersonic Aerothermodynamics*, ISBN 0-471-51093-9, Wiley, New York, 1990.

[10]Gokcen, T., "Computation of Hypersonic Low Density Flows with Thermochemical Nonequilibrium," Ph.D. Dissertation, Stanford Univ., Stanford, CA, 1989.

[11]Lumpkin, F., "Development and Evaluation of Continuum Models for Translational-Rotational Nonequilibrium," Ph.D. Dissertation, Stanford Univ., Stanford, CA, 1990.

[12]Millikan, R. C., and White, D. R., "Systematics of Vibrational Relaxation," *Journal of Chemical Physics*, Vol. 39, No. 12, 1963, pp. 3209–3213.

[13]Davies, C., and Venkatapathy, E., "A Simplified Self-Adaptive Grid Method, SAGE," NASA TM 102198, Oct. 1989.

[14]Jeans, J. H., *The Dynamic Theory of Gases*, Cambridge University Press, 1904.

[15]Parker, J. G., "Rotational and Vibrational Relaxation in Diatomic Gases," *Physics of Fluids*, Vol. 2, No. 4, 1959, pp. 449–462.

[16]Breshears, W. D., and Bird, P. F., "Effect of Oxygen Atoms on the Vibrational Relaxation of Nitrogen," *Journal of Chemical Physics*, Vol. 48, No. 10, 1968, pp. 4768–4773.

[17]Taylor, R. L., Camac, M., and Feinberg, R. M., "Measurements of Vibration-Vibration Coupling in Gas Mixtures," *Eleventh Symposium (International) on Combustion Papers*, 1967, pp. 49–65.

[18]McNeal, R. J., Whitson, M. E., Jr., and Cook, G. R., "Quenching of Vibrationally Excited N_2 by Atomic Oxygen," *Chemical Physics Letters*, Vol. 16, No. 3, 1972, pp. 507–510.

[19]Kiefer, J. H., and Lutz, R. W., "The Effect of Oxygen Atoms on the Vibrational Relaxation of Oxygen," *Proceedings of the 11th Symposium (International) on Combustion*, 1967, pp. 67–76.

[20]Wray, K., "Shock-Tube Study of the Vibrational Relaxation of Nitric Oxide," *Journal of Chemical Physics*, Vol. 36, No. 10, 1962, pp. 2597–2603.

[21]Moreau, S., Chapman, D. R., and MacCormack, R. W., "The Effect of Rotational Relaxation and Approximate Burnett Terms on Hypersonic Flow-Field Radiation at High Altitudes," AIAA Paper 91-1702, June 1991.

[22]Crosley, D. R., Eckstrom, D. J., Smith, G. P., Jusinski, L. E., Meier, U. E., and Raiche, G. A., "Energy Transfer and Kinetics in Radiating, Shock-Heated Air," Stanford Research Inst. International, Rept. MP91-099, April 1991.

[23]Kee, R. J., Miller, J. A., and Jefferson, T. H., "CHEMKIN: A General-Purpose, Problem-Independent, Transportable, Fortran Chemical Kinetics Code Package," Sandia Rept. SAND80-8003·UC-4, 1988.

[24]Bortner, M., and Kummler, R., "The Chemical Kinetics and the Composition of the Earth's Atmosphere," G. E. Rept. GE-9500-ECS-SRI, 1968.

[25]Baulch, D. L., Drysdale, D. D., Home, D. G., and Lloyd, A. C., "Evaluated Kinetic Data for High Temperature Reactions," *Homogeneous Gas Phase Reactions of the H_2-O_2 System*, Butterworth, Vol. 1, 1972, ISBN 0 408 70346 6.